Computational Design Strategy to Improve RF Heating Uniformity

J. Allison, J. Pearce, J. Beaman, C.C. Seepersad

Abstract

Recent work has demonstrated the possibility of selectively sintering polymer powders with radio frequency (RF) radiation as a means of rapid, volumetric additive manufacturing. Although RF radiation can be used as a volumetric energy source, non-uniform heating resulting from the sample geometry and electrode configuration can lead to adverse effects in RF-treated samples. The focus of this work is to present two approaches for improving the RF heating uniformity with the goal of developing an RF-assisted additive manufacturing process for thermoplastic polymers. Both techniques utilize COMSOL Multiphysics® to predict the temperature rise during simulated RF exposure for different sample geometries. The effectiveness of each approach is evaluated by calculating the uniformity index, which provides an objective metric for comparing the heating uniformity across the simulations. The first approach implements an iterative heuristic tuning strategy to functionally grade the electrical conductivity within the sample. The heuristic tuning method is shown to improve the uniformity index for several test geometries. In the second approach, the heating uniformity is improved by reorienting the electrodes during the heating stage such that the electric field is applied in two directions. Lastly, the greatest improvement in heating uniformity is demonstrated by combining the approaches and functionally grading the samples while using multiple electrode orientations.

1 Introduction and Background

Most additive manufacturing (AM) techniques for thermoplastic polymers rely on layer-wise heating strategies where the polymer is melted and re-solidified at each layer during the build, contributing to lengthy processing times. Radio frequency additive manufacturing (RFAM) is a volumetric approach that seeks to improve the process speed by delivering energy in the form of RF radiation. Insulating polymer powders can be combined with an electrically conductive dopant to achieve selective, volumetric heating in a powder bed subjected to RF radiation. The feasibility

of a radio frequency — assisted additive manufacturing process for thermoplastic polymers was demonstrated in previous work where mixtures of polymer and graphite powders were fused using RF radiation as the sole energy source [1]. However, heating uniformity issues in RF applications present a challenge to the development of a radio frequency additive manufacturing process because they place limitations on the geometries that can be created. The presence of local hot and cold areas negatively impacts the resulting fused geometry, causing unintended warping and lack of fusion in certain regions of the part. One of the primary advantages of additive manufacturing is the production of complex geometries that cannot be manufactured using conventional methods; therefore, techniques to improve RF heating uniformity are necessary in the development of this new process.

Although RF radiation offers greater heating uniformity than other forms of radiation such as microwaves, non-uniform heating can still occur. Uneven heating can arise from the physical properties of the material such as the geometric, electrical, and thermal attributes as well as the properties of the RF system including the electrode spacing and engineering design of the apparatus [2]. Non-uniform heating for RF applications has been studied extensively through simulation and experimentation, and several attempts have been made to improve the uniformity by rotating the sample [3,4], rounding corners [5], pulsing the energy input, and artificially thickening the cold regions [6].

The focus of this work is to develop computational models that represent the selectively doped powder beds to enable the prediction of temperature rise and phase change behavior during RF radiation exposure. Using the models, two solutions are proposed for improving the heating uniformity within the parts. In the first approach, the electrical conductivity is functionally graded in an iterative strategy to mitigate the geometric effects on the heating uniformity. Most of the research in this area has been applied to foods or products with predefined material properties, and the effect of locally tuning dielectric properties has received little attention [7]. The second approach seeks to improve the heating uniformity by applying the electric field in multiple discrete

orientations during the simulated RF exposure. This work differs from previous efforts aimed at improving the RF heating uniformity because the AM application facilitates local tuning of electrical properties, and the use of discrete electric field orientations enables greater complexity in the simulated geometries.

2 Methodology

Analytical solutions to RF heating problems are often too complex to calculate and require numerical approaches and finite element analyses to solve [8]. Therefore, COMSOL Multiphysics® was used to represent the doped powder beds in simulations of the RFAM process. The region corresponding to the part was prescribed the electrical properties of the doped powder while the surrounding powder bed was modelled as an electrical insulator. The RF heating simulations were comprised of an electric component as well as a thermal component. COMSOL® version 5.3a was used in conjunction with the supplemental AC/DC and Heat Transfer modules to predict the temperature rise in the simulations. Figure 1 shows a representation of the simulated domains in COMSOL® with the doped geometry in the center. The voltage and convection boundary conditions are displayed. The models were simulated in a time-dependent, transient study with a prescribed radiation exposure time.

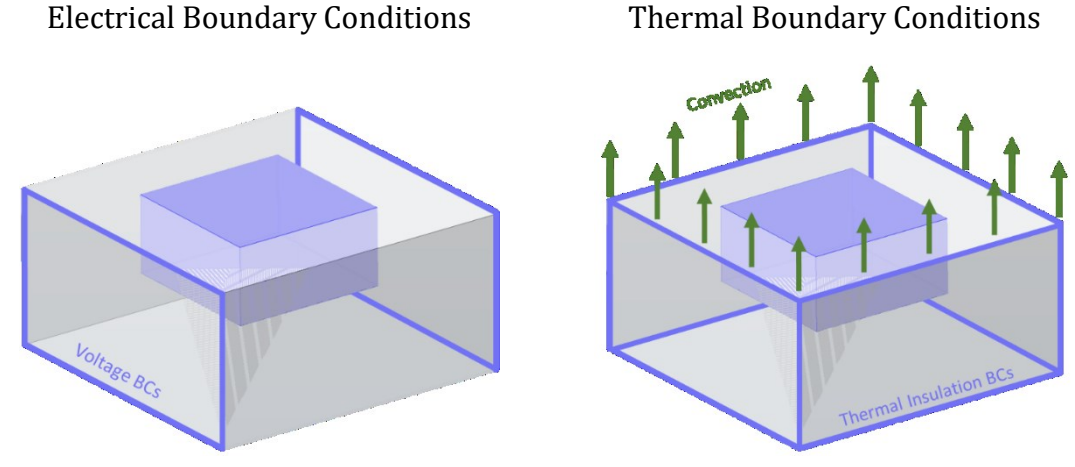


Figure 1 Simulated domains in COMSOL®. The electrodes are represented by voltage boundary conditions. The doped region and surrounding region are distinguished by prescribing electrical properties corresponding to the doped and virgin nylon powders, respectively.

2.1 AC/DC Model Parameters

The applicator and virgin powder bed were modelled as a rectangular cavity, and the electrodes were simulated as voltage boundary conditions on opposite faces of the applicator. For RF-assisted AM applications, the size of the applicator is much smaller than the radiation wavelength, and therefore the electroquasistatic (EQS) approximation is valid for the simulations. Under the EQS approximation, wave propagation effects and magnetic field contributions to heating can be ignored [9]. Eliminating the wave effects greatly reduced the computational complexity of the RF heating simulations. By considering the voltage as the primary input, the electroquasistatic approximation was enforced. The remaining four faces of the applicator were prescribed electrically insulating boundary conditions in which the current density normal to the surface was zero, depicted in Equation 1.

$$n \cdot \mathbf{J} = 0 \tag{1}$$

For the electric component in the simulation, three primary relationships were used to determine the heat generation. Gauss' Electric Law in semiconducting media (Equation 2), the electric field definition (Equation 3), and the right-hand-side of Ampere's Law in point form (Equation 4) were applied to determine the current density (J), electric field strength (E), and electric potential (V) [9]. The inputs to the electrical model were the peak root mean square potential difference at the electrodes (V_0), frequency (ω), and the electrical properties of the doped and virgin powder regions (σ and ε_r). In Equation 4, ε_0 represents the permittivity of free space with a value of 8.85×10^{-12} F/m.

$$\nabla \cdot \boldsymbol{J} = 0 \tag{2}$$

$$\mathbf{E} = -\nabla V \tag{3}$$

$$\mathbf{J} = (\sigma + j\omega\varepsilon_0\varepsilon_r)\mathbf{E} \tag{4}$$

The doped geometry was placed in the center of the cavity with corresponding electrical properties. From the current density and electric field, the resistive power density (Q_{rh} , W/m³) was

determined according to Equation 5. The power density represented the volumetric energy loss within the doped region and provided a measure of the electric field heating.

$$Q_{rh} = Re\{ \boldsymbol{J} \cdot \boldsymbol{E} \} \tag{5}$$

The properties in the electrical simulation were derived from impedance spectroscopy measurements detailed in previous work [1]. The values for the model parameters are given in Table 1. The electrical properties in the models did not include a dependence on temperature. Previous studies have shown the conductivity of graphite/polymer composites to decrease with increasing temperature, possibly due to the disruption of conductive pathways through thermal expansion during heating [10]. Further testing is required on the nylon and graphite composites to confirm the temperature dependence and incorporate it into the simulation models.

Property Symbol Value Electrode Voltage V_0 1200 [V]Frequency ω $1.7x10^{8}$ [rad/s] f 27.12 [MHz] Effective Virgin 0 [S/m] σ_{eff} Conductivity Doped 0.04 [S/m]Relative Virgin 2 εr Permittivity Doped 13.8

 Table 1
 Electrical properties used in simulation for doped and virgin powder regions

2.2 Heat Transfer Model Parameters

The temperature rise in the simulations was calculated in the thermal component of the model according to Equations 6 and 7. The electric and thermal modules were coupled together through the resistive power density as depicted in Equation 6. The inputs to the thermal model were density (ρ) , specific heat (C_p) , and thermal conductivity (k), and temperature was the output [11].

$$\rho C_p \frac{\partial T}{\partial t} + \nabla \cdot q = Q_{rh} \tag{6}$$

$$q = -k\nabla T \tag{7}$$

Depicted in Figure 1, thermal insulation boundary conditions were prescribed to each external face with the exception of the top face in which thermal convection was considered. The thermal insulation prevented outward heat flux according to Equation 8, while the convection heat flux followed Equation 9.

$$-n \cdot q = 0 \tag{8}$$

$$-n \cdot q = h(T_{ext} - T) \tag{9}$$

The thermal models also included phase transition between the solid and liquid phases. COMSOL® uses an apparent heat capacity formulation to model phase change by assuming a smooth transition between phases across a predefined temperature interval. Outside the temperature window, either the solid or liquid phase properties were used depending on whether the temperature was above or below the transition region. Within the interval, the material was assigned mixed properties according to the smooth transition function (θ) that represented the fraction of each phase at a given temperature. The thermal properties were calculated according to Equations 10-13, where the heat capacity (C_p) incorporated the latent head of fusion (L) to compensate for energy losses during the phase transition. The subscripts S and L refer to the properties for the solid and liquid phases, respectively.

$$\rho = \theta \rho_S + (1 - \theta)\rho_L \tag{10}$$

$$k = \theta k_S + (1 - \theta)k_L \tag{11}$$

$$\alpha_m = \frac{1}{2} \left[\frac{(1-\theta)\rho_L - \theta\rho_S}{\theta\rho_S + (1-\theta)\rho_L} \right] \tag{12}$$

$$C_p = \frac{1}{\rho} \left[\theta \rho_S C_{p,S} + (1 - \theta) \rho_L C_{p,L} \right] + L \frac{\partial \alpha_m}{\partial T}$$
 (13)

The thermal properties used in the simulations were taken from values found in literature and are given in Table 2. One of the simplifications in the models was that only the thermal properties of the polymer powder were considered, and no distinction was made between the thermal properties of the virgin and doped regions. In omitting the contribution from the dopant, the melting characteristics of the polymer powders were prioritized. The addition of a graphite

dopant has been shown to increase the thermal conductivity of polymer mixtures. However, graphite powders have a wide range of reported thermal conductivities, and the values for dry powder mixtures have not been widely studied [12]. Without direct measurement of mixture properties, only the polymer properties were considered in the simulations. Further, as RF radiation heats the volume simultaneously, thermal conductivity plays a smaller role in the heating of the mixtures [13]. The models allowed thermal conduction into the surrounding virgin powder bed and sintering beyond the domain of the doped region. An opportunity for future work would be direct thermal property measurement of the nylon/graphite composites to enhance the simulations.

Table 2 Thermal properties used in the simulations, including phase change. The values corresponded to pure nylon 12 powder and were taken from sources in literature.

Property	Symbol	Value			Reference
Convection Coefficient	h		25	$[W/m^2K]$	[14]
Melting Point	$T_{S \to L}$		180	[°C]	[15]
Latent Heat	$L_{S \to L}$		96.7	[kJ/kg]	[16]
Thermal Conductivity	\mathbf{k}_{S}	Solid	0.1	[W/mK]	[17]
	\mathbf{k}_{L}	Liquid	0.26	[W/mK]	[17]
Density	$ ho_{ ext{S}}$	Solid	490	$[kg/m^3]$	[14]
	$ ho_{ m L}$	Liquid	1010	$[kg/m^3]$	[14]
Heat Capacity	$C_{p,S}$	Solid	1287	[J/kgK]	[18]
	$C_{\mathrm{p,L}}$	Liquid	2500	[J/kgK]	[16]

2.3 Dependence of Heating Uniformity on Doped Geometry

The COMSOL® models were used to predict the temperature rise due to RF radiation for various geometries. Figure 2 gives the temperature profiles at the center cross section for spherically and cubically doped regions. The white lines in the figures correspond to the electric field within the powder bed. Although the applied electric field is uniform, the presence of the doped geometry causes distortions in the field as it interacts with the higher conductivity in the region. According to the power loss relationship described by Equation 5, a non-uniform electric field gives rise to non-uniform power loss within the material. The electric field is uniform within a spherical geometry, as evidenced by the parallel, equally spaced field lines in Figure 2a. The heating within the sphere is also uniform as a result of the uniform electric field. However, when

the geometry is changed to a cube, as in Figure 2b, the electric field within the conducting region becomes curved with local concentrations in the field lines. Local hot and cold regions arise from the non-uniform electric field in the cube. Non-uniform heating is expected for any geometry that deviates from spherical. The presence of sharp corners and flat faces are particularly prone to causing electric field concentrations within the doped region.

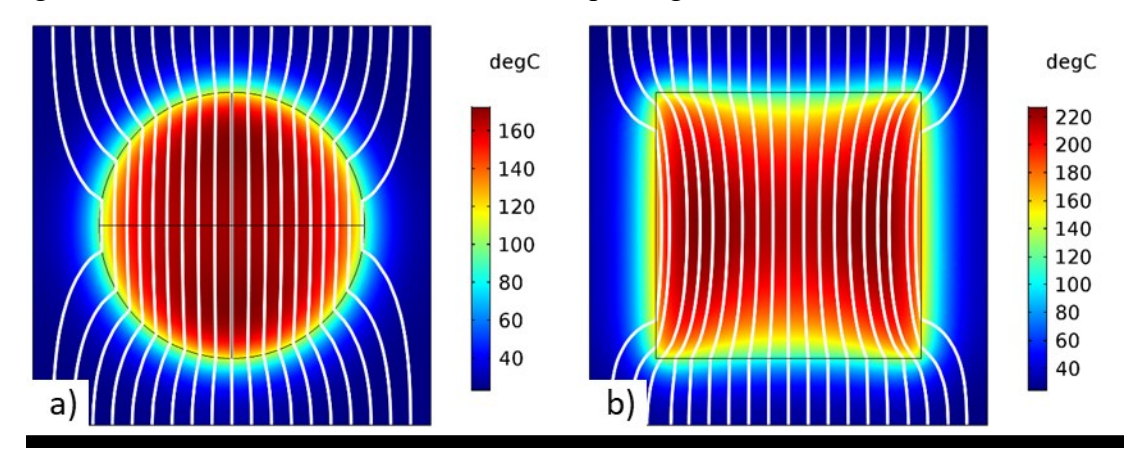


Figure 2 Temperature distribution at the center cross section for a sphere (a) and cube (b). The white lines in the image correspond to the electric field lines in the powder bed.

The computational models were validated against RF heating experiments from previous work that used 42 µm nylon 12 powder supplied by Arkema and 44 µm graphite powder supplied by Loud Wolf to create mixtures containing 30% graphite by weight [1]. The simulated surface temperatures compared to the experimentally measured IR surface temperatures for square, circular, and rectangular doped regions are given in Figure 3. Comparing the temperatures at three locations for each of the geometries shows close agreement between the models and the experiments. Another point of agreement is in the presence of hot spots on the sides for the square and rectangle; however, the shape of the temperature distributions differs between the simulations and experiments. The local hot spots in the IR images are much more exaggerated than the simulations suggest, but the general temperature distributions are similar.

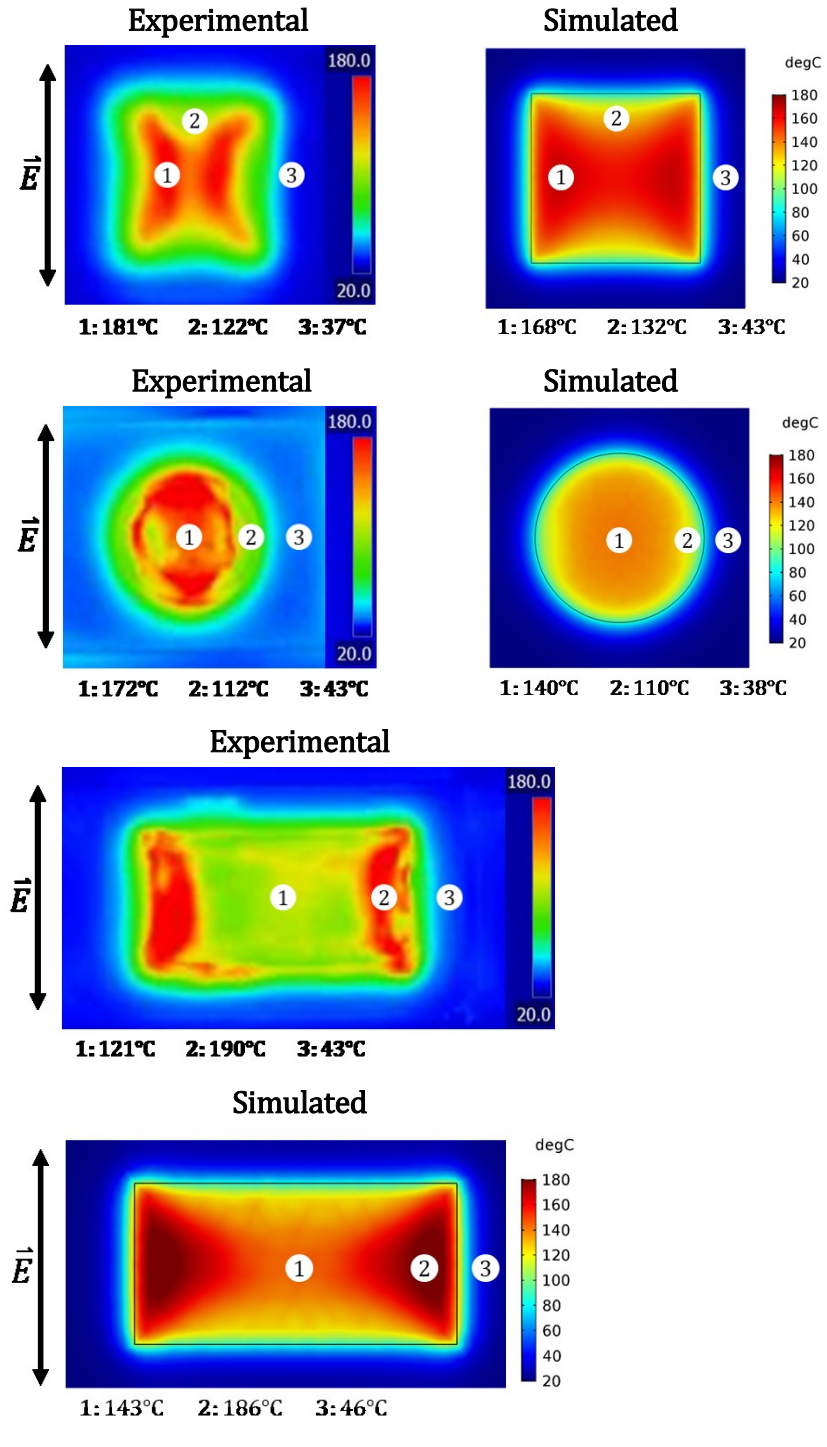


Figure 3 Comparison between the simulated surface temperature and the experimentally measured surface temperature for doped regions with square, circular, and rectangular cross sections. The numbers in the figure correspond to the temperature measurement locations.

The geometry of the sintered parts can be approximated by considering the phase of the powder bed at the end of the simulation. Although the models do not account for cooling effects,

the part geometry can be predicted by representing the volume of the domain that is in the liquid phase after the simulated RF heating. Due to the steep thermal gradients at the phase transition boundary, accurate predictions often require an extremely fine FEA mesh and can be computationally expensive to solve [19]. The phase change parameter in COMSOL® (θ) is represented by a continuous value between 0 and 1 where the material at a given location is entirely solid when $\theta=\theta$, entirely liquid when $\theta=1$, and has mixed properties between the two domains. Smaller windows can produce sharp transitions in phase but with an added computational complexity from the necessary mesh refinement. To reduce the computational expense, a transition window of 60°C is used for the RF simulations where phase transition begins at a temperature of 120°C and ends at 180°C.

The geometry is approximated by displaying only the volume in which the phase change parameter is equal to one, indicating that the temperature exceeds the melting temperature of the polymer. The thermal model is improved by incorporating phase transition by considering the energy required to fuse the polymer (latent heat). Figure 4 shows the comparison between the geometry predictions from the simulations with the experimentally fused parts for the circular, square, and rectangular cross sections. The geometric predictions successfully capture the main trends in the fused parts. Namely, the elongation of the cylinder in the direction of the applied electric field and the thickening of the sides in the square and rectangular parts show agreement between the simulation models and the fused geometries.

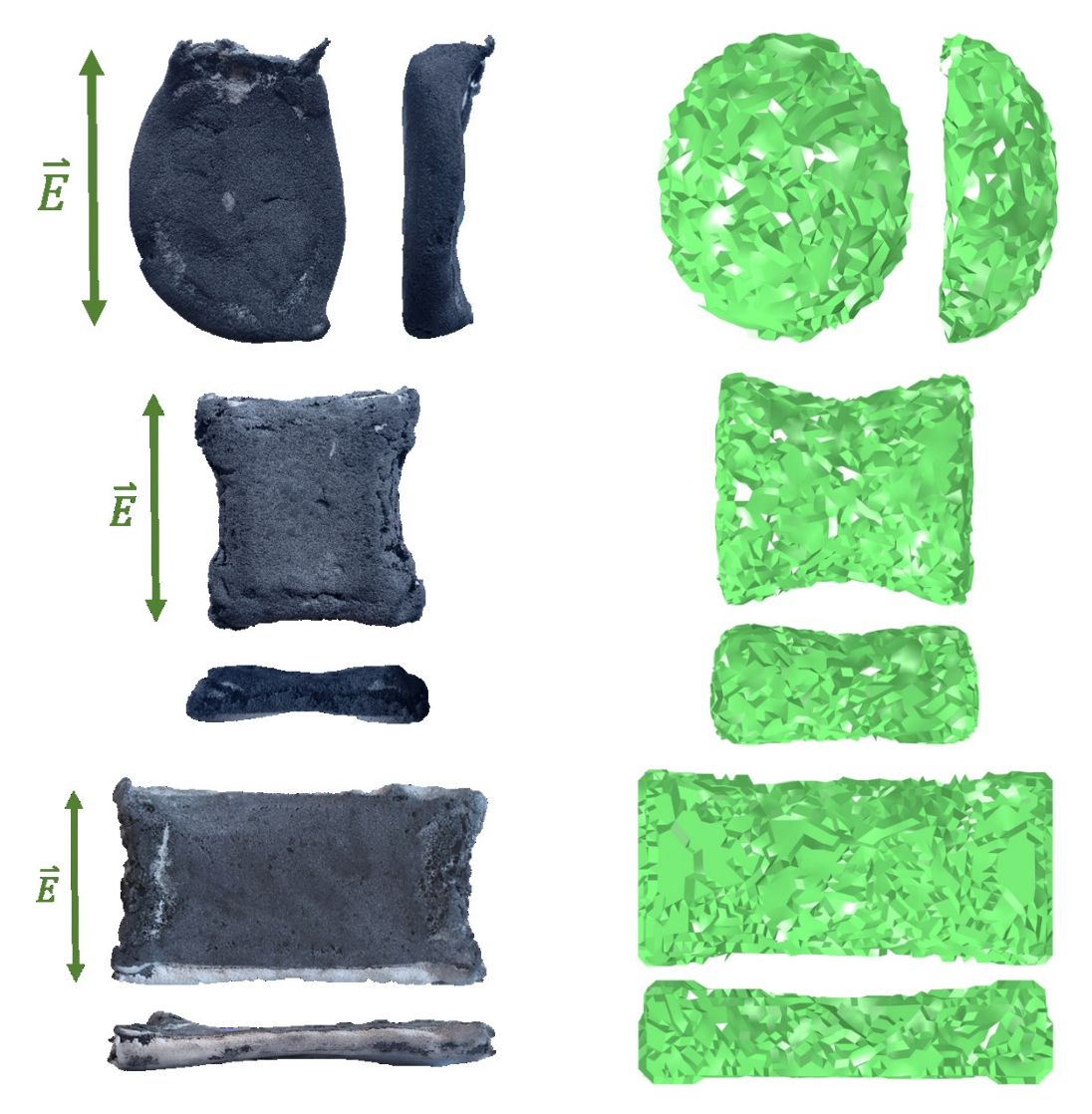


Figure 4 Comparison between experimental (left) and simulated geometry (right) by considering the volume in the liquid phase at the end of the simulation run

The geometric dependence of heating uniformity on the doped geometry must be addressed to enable the creation of parts with arbitrary geometries in an RF-assisted AM process. Previous studies have proposed solutions to improve the heating uniformity in RF applications such as modifying the material and electrode geometries [5] and adding sacrificial material above cold regions to artificially thicken them [6]. In most cases, the electrical properties of the substance being heated are fixed, and the geometry can be modified to some extent to improve heating uniformity. In the case of graphite-doped polymer parts, the geometry is fixed, but the electrical properties can be varied by adjusting the amount of dopant throughout the part. In this way, the

dopant can be functionally graded within the powder bed. Computational methods are needed to determine the correct grading within the part to improve the heating uniformity.

2.4 Computational Approaches to Functionally Grade Electrical Conductivity

The topic of functionally grading materials is an active research endeavor in multi-material AM processes, where two materials are combined in such a way that local flexibility or rigidity can be achieved within a single part [20]. This principle was adapted for the RF-assisted AM process to functionally grade the graphite concentration within the nylon composites to improve the heating uniformity and enable the fabrication of complex structures. The COMSOL® models were used in a computational design strategy to functionally grade the dopant.

Topology optimization techniques using the SIMP approach are widely used in structural applications [21–24]. Such techniques could be adapted to determine the required grading, however, they rely on spatial gradients to converge on a solution. Analytical relationships describing the tradeoff between geometry and heating uniformity are unavailable for arbitrary shapes, and so RF problems must be treated as black boxes in which the mapping from input to output is unknown. In the absence of analytical gradients, finite differencing approaches can be used to calculate the gradients at each iteration. However, calculating gradients in a 3D finite element model with the finite difference approach creates an additional computational expense. The number of required function calls per iteration is proportional to the number of nodes in the FEA mesh, and the problem quickly becomes intractable. Therefore, traditional optimization techniques are not the preferred methods for functionally grading the doped powder beds.

Instead of using topology optimization to tune the electrical conductivity, the heating uniformity was improved by applying a heuristic to adjust the conductivity. The basis for the heuristic was that the conductivity should be raised in regions where the local temperature is lower than a specified target temperature and lowered when the temperature is higher. The heuristic was validated by performing simulations in COMSOL® in which the electrical conductivity was adjusted, and the average temperature recorded after two minutes of simulated RF exposure. The

normalized temperature rise as a function of electrical conductivity is shown in Figure 5. The maximum value for the trend occurred at an electrical conductivity of 0.0425 S/m, after which the temperature rise began to decrease with increasing conductivity. The simulations showed the heuristic to be valid as long as the electrical conductivity was kept below 0.0425 S/m beyond which an increase in conductivity led to a decrease in temperature rise due to a reduction in the RF penetration depth at higher levels of conductivity. RF heating experiments showed a similar trend where the electrical conductivities of the powder mixtures at the peak temperature rise were between 0.0423 S/m and 0.0862 S/m corresponding to graphite concentrations of 32.5% and 35% by weight, respectively.

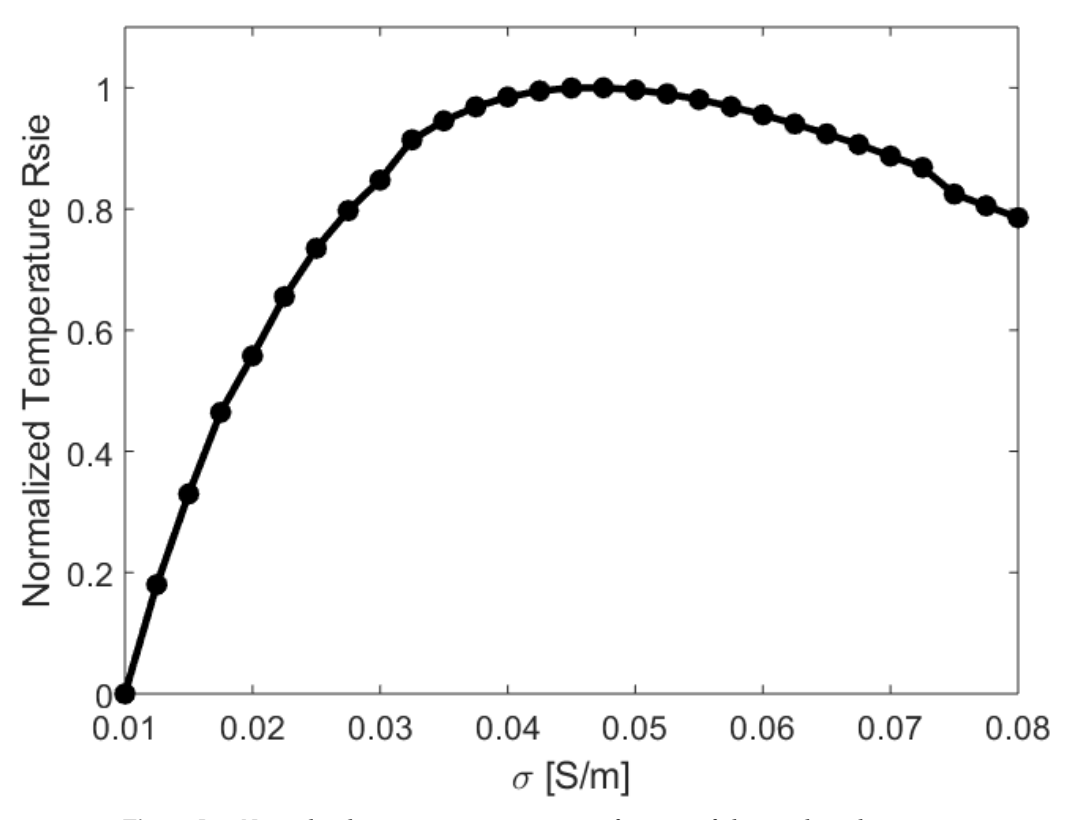


Figure 5 Normalized average temperature as a function of electrical conductivity.

To functionally grade the electrical conductivity, the heuristic was applied in an iterative scheme at each of the nodal locations in the finite element mesh, and the values were applied to the elements using an internal interpolation algorithm in the COMSOL® solver. Starting with

uniform electrical conductivity, the conductivity for the next iteration was adjusted based on the current node temperature relative to a target temperature. A flowchart of the heuristic tuning procedure is shown in Figure 6, and the heuristic is defined in Equation 15. For a given iteration, the temperature at each mesh node (denoted by i) was queried, and the conductivity was adjusted according to Equation 15 where σ_i and σ_{i+1} corresponded to the conductivity for the current and next iteration, respectively. The size of the adjustment was determined by the proportionality constant (K_i) and the difference between the nodal temperature (T_i) and target temperature (T_{target}) . The temperature difference term (ΔT_i) was normalized to the maximum observed difference (ΔT_{max}) , penalizing nodes with larger errors by applying a stronger correction. The sign of ΔT_i implicitly accounted for the direction in which the heuristic was applied by reducing the conductivity when the target temperature was greater than the nodal temperature. If the temperature at a given node passed through the target temperature between iterations, indicated by a sign reversal in ΔT_i , the proportionality constant at the node was halved for the next iteration. In this way, the nodal temperature converged on the target temperature. The heuristic tuning procedure was repeated until either the maximum number of iterations was met or the maximum temperature difference fell below a predetermined threshold.

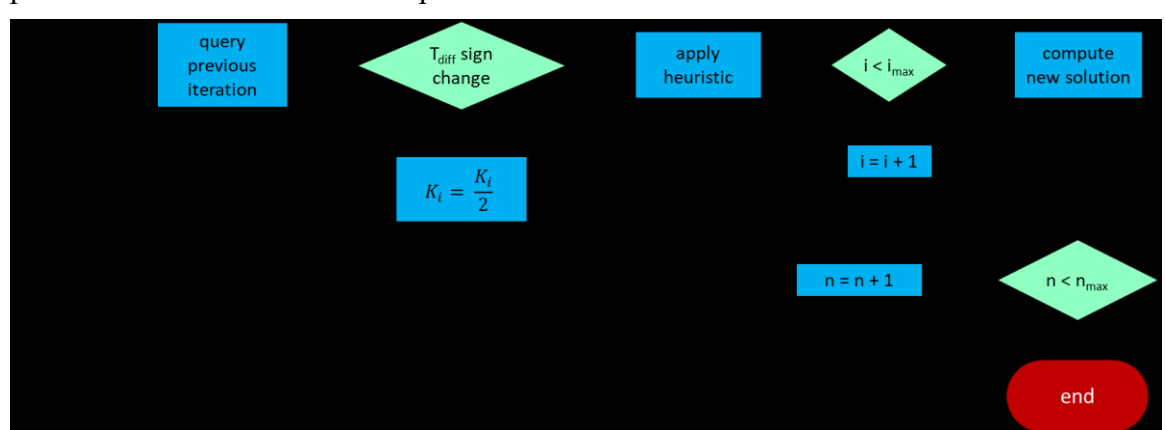


Figure 6 Flowchart describing how the heuristic tuning method was applied to the simulation results. The variables n and n_{max} represented the current and maximum iteration, while i and i_{max} corresponded to the current and maximum number of nodes. The proportionality constant, K, was uniquely assigned to each node for every iteration.

$$\sigma_{i+1} = \sigma_i + K_i * \frac{\Delta T_i}{\Delta T_{max}} \tag{15}$$

$$\Delta T_i = T_{target} - T_i \tag{16}$$

$$\Delta T_{max} = \max(T_{target} - T_i) \tag{17}$$

The main simplification in the heuristic method was that each mesh node was treated as fully independent of the neighboring nodes. Considering the nodes to be independent, however, enabled the heuristic to be applied at every element simultaneously for a given iteration. In this way, the electrical conductivity was incrementally adjusted at each mesh node location after a single function call to the finite element simulation. By comparison, optimization using finite differencing would have required n+1 function calls for n mesh nodes in a given iteration to tune the conductivity. While the heuristic tuning method did not guarantee optimal solutions, the computational expense was dramatically reduced compared with SIMP methods by eliminating the need to calculate gradients at each iteration. In most cases, the tuning procedure converged on a solution after only 15 function calls to the COMSOL® simulation, making the process tenable on a standard desktop computer.

In typical FEA settings, properties are applied to the elements in the mesh, and the results are calculated at the nodes. However, material property definitions in COMSOL® are decoupled from the FEA mesh, and spatial variation of the properties was achieved by assigning unique conductivity values to designated coordinates throughout the domain. COMSOL® then used a linear interpolation scheme between the specified coordinates to assign the properties to the elements when solving. To ensure the electrical conductivities were defined on a similar length scale to the elements in the FEA mesh, the coordinates of the mesh nodes were used as the locations for the property assignment. Although it is uncommon to define properties at nodal locations, the interpolation mechanism in the COMSOL® solver compensated for the discrepancy. A uniformity index was used to evaluate the effectiveness of the tuning process. The index, defined in Equation 18, considers the temperature difference across the entire part volume and is useful for making direct comparisons for a given model configuration [25]. The heating uniformity was governed by the temperature at each FEA node (T), the average temperature across the part domain (T_{av}), and the volume of the part domain (T_{av}). An initial temperature ($T_{initial}$) of 20°C was prescribed

in the calculations, and the remaining quantities were computed in COMSOL® using a fourth order numerical integration technique across the FEA nodes.

$$UI = \frac{\frac{1}{V} \int_{V} \sqrt{(T - T_{av})^2} dV}{T_{av} - T_{initial}}$$
(18)

Smaller values of the index indicate greater heating uniformity with a minimum value of zero to signify no temperature differences across the domain. The uniformity index calculations were carried out within the COMSOL® models and were restricted to the doped region only.

Before applying the heuristic tuning method, a convergence study was carried out to measure the effect of element size on the uniformity index in the FEA simulations. COMSOL® generated the mesh using five independent parameters that governed the element size, and the values of the parameters were sorted into different categories according to the COMSOL® algorithm for mesh refinement. To reduce the computational expense, the powder bed was given a coarser mesh than the doped region. This was a valid assumption when determining heating uniformity because uniformity index was calculated for the doped region only. The convergence study was conducted with a square prism geometry using tetrahedral elements to define the mesh. The dimensions of the doped region were 4x4x2 cm, and an example mesh is shown in Figure 7.

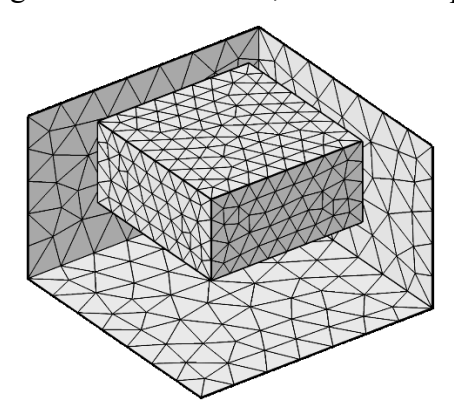


Figure 7 Example finite element mesh for RFAM simulations

The powder bed was assigned a "coarse" mesh according to the COMSOL® mesh refinement categories, while the elements in the doped region were varied from "extremely coarse" to "very fine." The uniformity index as a function of element size is shown in Figure 8. The x axis

represents the number of elements used in the simulation, where higher values correspond to a finer mesh.

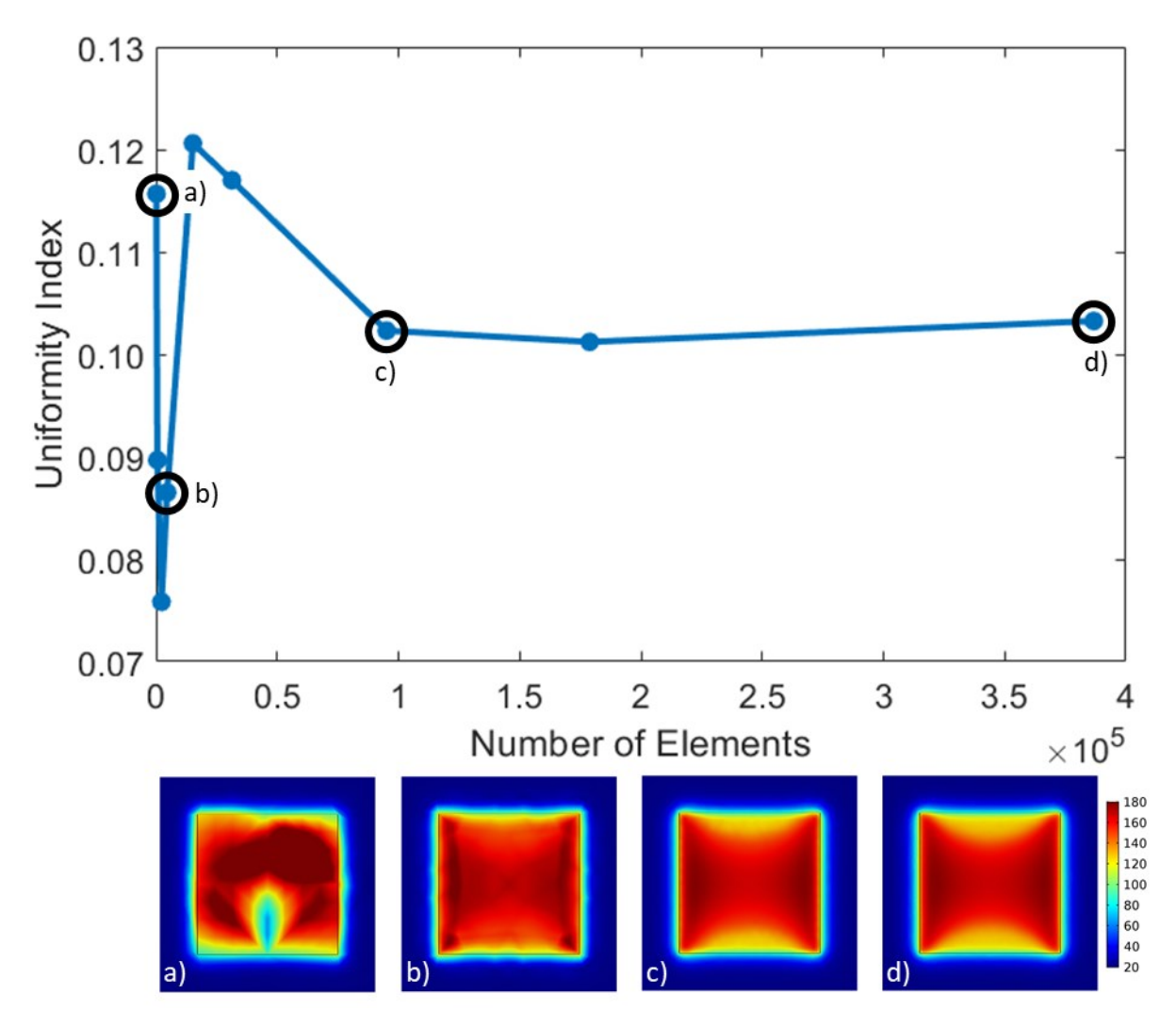


Figure 8 Mesh convergence for square prism. The x axis represents the number of elements in the simulation where higher values correspond to a finer mesh.

The convergence study revealed large variations in the uniformity index for coarse meshes that stabilized as the mesh was refined. To balance computational time and model accuracy, the mesh size category corresponding to point c) in Figure 8 was used for the heuristic tuning simulations. The convergence study was intended to validate the meshing procedure in

COMSOL®, which used internal algorithms to optimize the five sizing parameters for a given refinement category. Different geometries may lead to different values for the five parameters.

3 Results

3.1 Heuristic Tuning Approach

The heuristic tuning method was applied to three geometries: a square prism, an equilateral triangular prism, and a thin ring. The simulated domains are shown in Figure 9 where the electrode locations with respect to the doped geometries are marked in purple. The dimensions of the chamber are 6.24x6.24x2.0 cm, and the dimensions of the different geometries are given in Figure 9. The model results were processed in a Matlab script that tuned the electrical conductivity at each iteration and ran the COMSOL® simulations using the *LiveLink for Matlab* tool. To start the tuning process, a constant electrical conductivity of 0.0425 S/m was prescribed to the doped region because it was associated with the highest degree of heating in the COMSOL® models. The simulations were carried out on a desktop computer with a 3.60 GHz processor, 16 GB of RAM, and 4 core CPU.

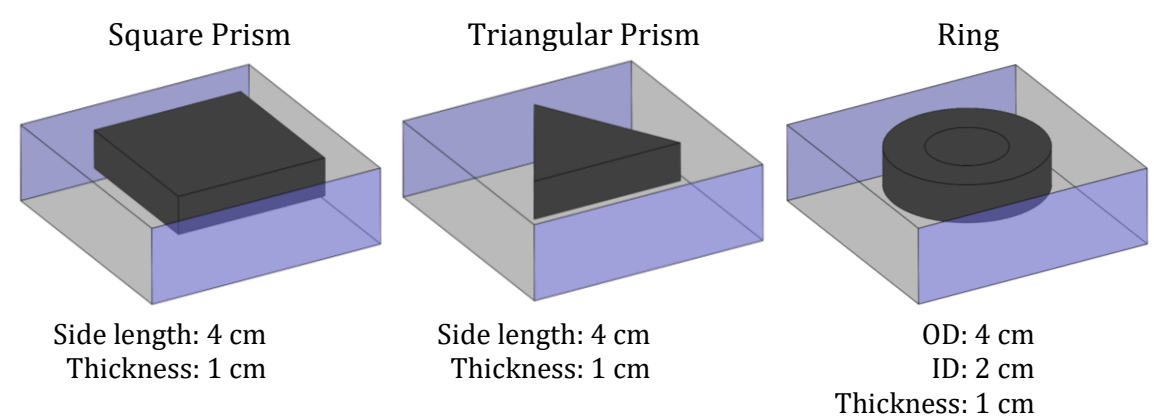


Figure 9 Simulated geometries used in the heuristic tuning method. The dark regions represent the doped geometry where the tuning was applied, and the location of the electrodes with respect to the geometry are indicated in purple. The dimensions of the chamber are 6.24x6.24x2.0 cm.

The maximum value of conductivity was prescribed as the initial conditions in the functional grading simulations, and so the process of tuning necessarily reduced the total effective conductivity within the part. For this reason, the tuned parts required a longer RF exposure time

to compensate for the reduction in the effective conductivity relative to the un-tuned, constant conductivity case. Figure 10 shows the predicted geometry, simulation RF exposure time, and uniformity index for the constant electrical conductivity case (left) and functionally graded conductivity (right) for the square prism. The tuning process was performed for 7 iterations completed in 553 seconds. The uniformity index was improved from 0.135 in the case of constant conductivity to 0.083 for the functionally graded conductivity. The predicted geometry also showed improvement after functional grading, where the curvature was reduced on the top and bottom faces.

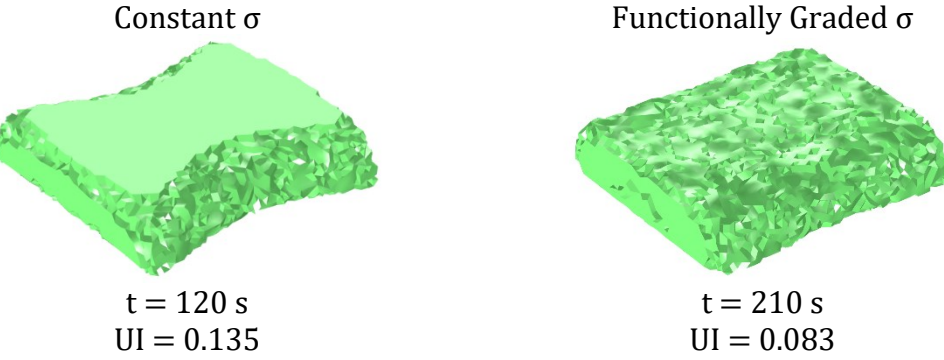


Figure 10 Comparison between constant conductivity (left) and functionally graded conductivity (right) for a 4x4x1 cm square prism, where t represents the simulated RF exposure time and UI is the uniformity index.

In a similar fashion, the tuning process was carried out for an equilateral triangle prism with a side length of 4 cm and depth of 1 cm. The comparison between the constant conductivity and functionally graded conductivity cases is given in Figure 11. For a constant conductivity, the electric field concentrated at the corner facing the electrodes and caused the region to sinter beyond the doped region. The uniformity index was improved from 0.262 to 0.094 after functionally grading the conductivity. The results are shown after 15 iterations of the heuristic tuning process and required 385 seconds to complete.

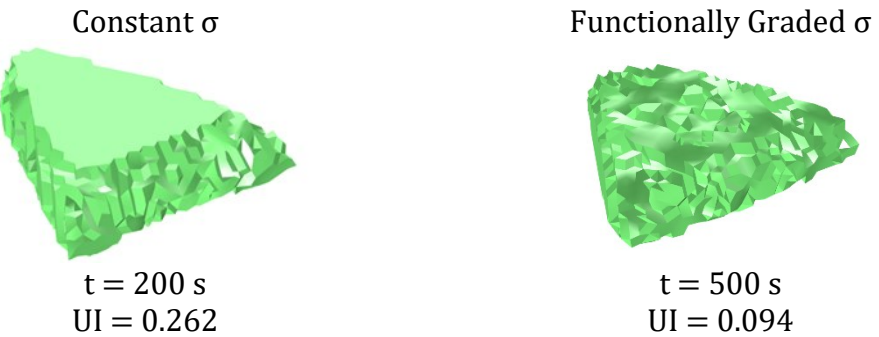


Figure 11 Comparison between constant conductivity (left) and functionally graded conductivity (right) for a triangular prism with a side length of 4 cm and 1 cm thickness, where t represents the simulated RF exposure time and UI is the uniformity index.

The heuristic tuning procedure was also tested on a thin ring with an inner radius of 1 cm, outer radius of 2 cm, and thickness of 1 cm. The comparison between the un-tuned and functionally graded electrical conductivities is shown in Figure 12. The geometry predictions showed substantial sintering in the sides of the ring in the direction of the applied electric field, and no sintering in the top and bottom regions for the constant conductivity case. After 15 iterations of functionally grading the electrical conductivity and 811 seconds of computational time, the uniformity index was improved from 0.263 to 0.077. Further, the geometry predictions for the tuned conductivity showed the formation of a single ring as opposed to the two separate sintered regions suggested by the constant doping simulation.

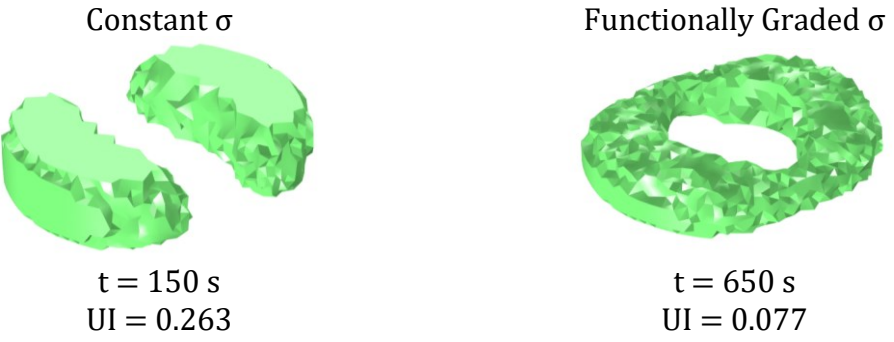


Figure 12 Comparison between constant conductivity (left) and functionally graded conductivity (right) for a 4 cm outer diameter, 2 cm inner diameter, and 1 cm thick ring, where t represents the simulated RF exposure time and UI is the uniformity index.

The functionally graded electrical conductivity distribution within the parts can provide additional insight into the interaction between the electric field and the doped geometry. Figure 13 shows the graded electrical conductivity at the center cross section of the square prism located 0.5

cm from the top and bottom faces. A majority of the tuning occurred along the perimeter of the doped region, while the conductivity did not vary significantly throughout the interior. The tuned conductivity in the interior was also notably low and nearly zero in most areas. The top and bottom regions were prescribed the highest conductivity, corresponding to the cold spots in the un-tuned case.

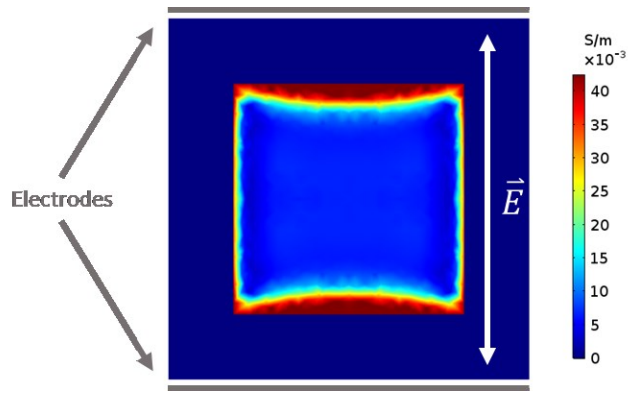


Figure 13 Spatially tuned conductivity for a 4x4x1 cm square prism at the center cross section.

The functionally graded conductivity at the center cross section of the triangular prism is shown in Figure 14. Similar to the square prism, the conductivity throughout the interior was nearly zero, and most of the tuning was concentrated around the perimeter. In the constant doping case, the electric field concentrated at the corner facing the electrodes which caused a sharp increase in the temperature. In response, the conductivity was reduced in the upper corner and increased in the other two corners during the functional grading process.

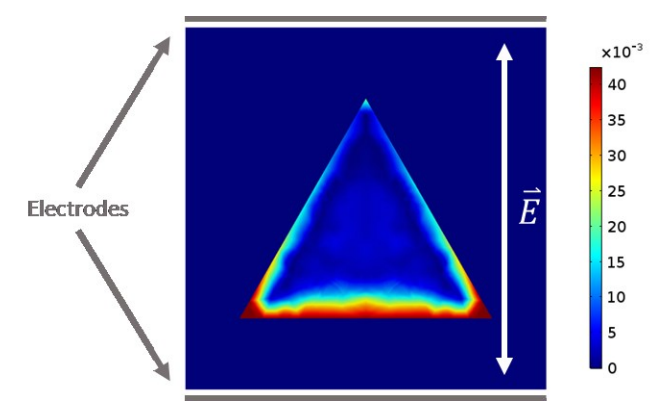


Figure 14 Spatially tuned conductivity for a triangular prism with a side length of 4 cm and depth of 1 cm at the center cross section.

Lastly, the functionally graded conductivity at the center cross section of the thin ring is given in Figure 15. The results were consistent with the previous two cases in which the conductivity within the interior was greatly reduced compared to the edges. The highest conductivity was prescribed to the top and bottom regions where the un-tuned predicted geometry showed a lack of fusion.

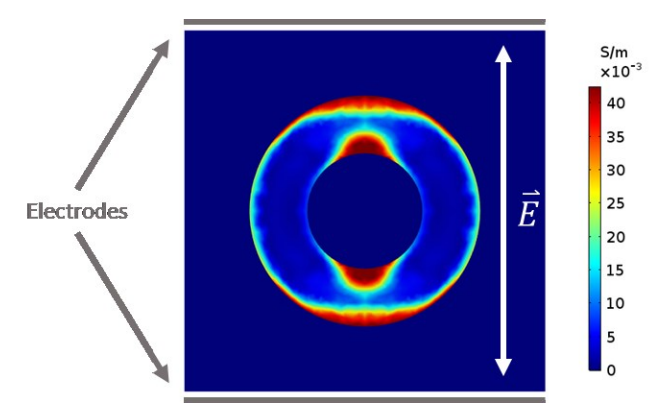


Figure 15 Spatially tuned conductivity for a 4 cm outer diameter, 2 cm inner diameter, and 1 cm thick ring at the center cross section.

3.2 Changing Electrode Configuration to Improve Heating Uniformity

In addition to functionally grading the electrical conductivity, modifying the electrode configuration was considered to improve the heating uniformity in the RF heating simulations. Birla et al. showed that rotating material with respect to the electric field in an RF applicator improved the heating uniformity in fruit [26]. However, simulating a rotating electric field can be difficult because the boundary conditions must also change at each time step, limiting the geometries that can be simulated [3]. Therefore, instead of modelling a continuously rotating powder bed, a two-stage heating process was considered in which the electrode configuration was modified sequentially during the simulation. The two-stage process consisted of activating opposing pairs of electrodes by changing the boundary conditions in the simulation as shown in Figure 16 for the thin ring. A portion of the simulation was conducted using the first configuration then switched to the second configuration for the remaining time steps.

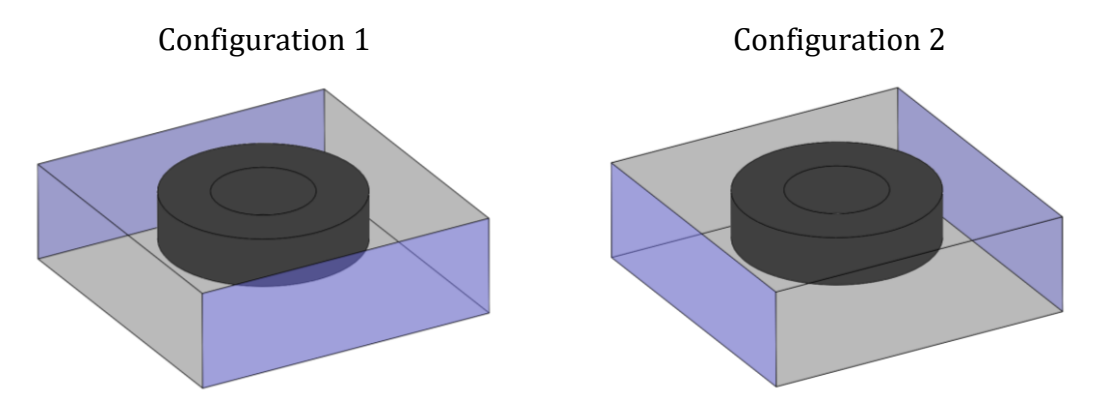


Figure 16 Electrode configurations for orientation-dependent simulations of a thin ring

Figure 17 shows the effect of applying multiple electrode configurations to the thin ring. The electrodes were activated for 75 seconds in the first configuration followed by 45 seconds in the second configuration. The heating times were asymmetrical because regions that were predominately heated in the first configuration began to cool as the second configuration was applied. The uniformity index for a constant electrical conductivity and single electrode configuration was 0.263 and improved to 0.109 with the two-stage process. The heating uniformity for multiple electrode configurations and a constant doping nearly matched the functionally graded uniformity index of 0.077 without implementing an iterative computational design strategy.

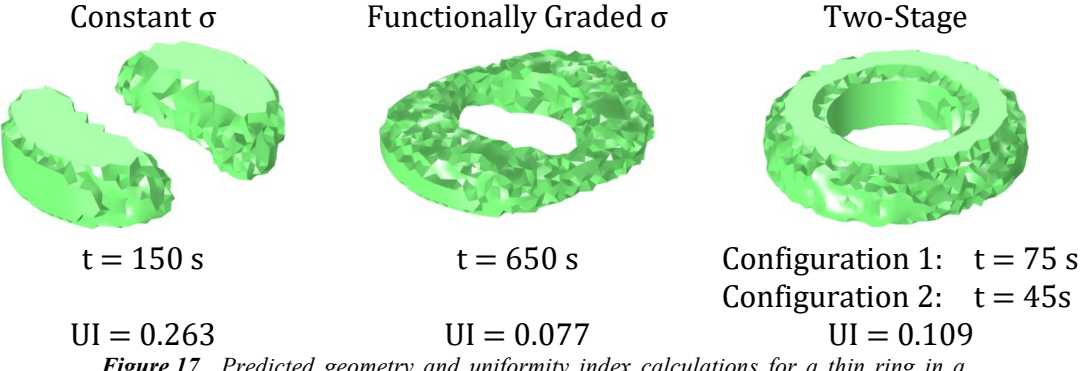
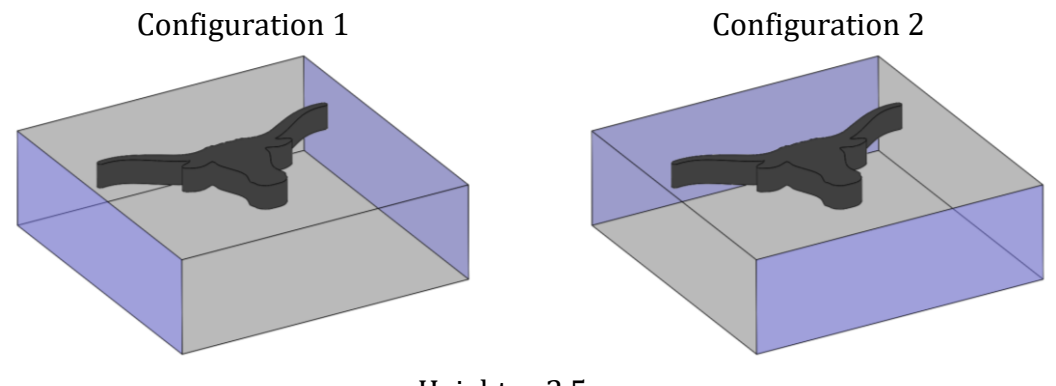


Figure 17 Predicted geometry and uniformity index calculations for a thin ring in a single electrode configuration with constant electrical conductivity (left), single electrode configuration with functionally graded electrical conductivity (middle), and constant electrical conductivity with multiple electrode configurations (right)

With the successful application of the two-stage heating method on the thin ring, the process was tested on a more complex geometry. With a large aspect ratio and detailed features, a

longhorn head was selected as the representative geometry. The two electrode configurations used in the simulations are shown in Figure 18.



Height: 2.5 cm Width: 5 cm Thickness: 0.5 cm

Figure 18 Electrode configurations for orientation-dependent simulations of a longhorn head. The height, width, and thickness correspond to the bounding dimensions of the longhorn head geometry.

Figure 19 shows the predicted geometries and uniformity index values for each electrode configuration as well as the combined two-stage case. For the first configuration, nearly all the fusion occurred in the horn region, while the predicted geometry for the second configuration showed fusion only in the head region. By implementing the two-stage process, the effects of the individual configurations were superimposed to produce a closer resemblance to the desired geometry. The uniformity index in the combined case was only slightly lower than in the second configuration but captured more detail in the predicted geometry. The smaller degree of heating in the horn region for configuration 2 had less of an effect on the uniformity index because the horns represented a smaller proportion of the part volume. The two-stage heating process improved the heating uniformity for the longhorn, but it was unable to resolve some of the finer details and curvature present in the desired part.

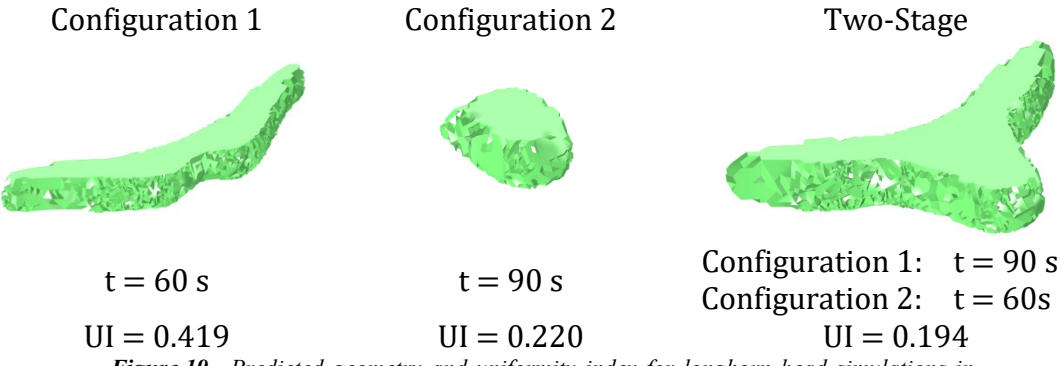


Figure 19 Predicted geometry and uniformity index for longhorn head simulations in each electrode configuration as well as the two-stage combined configuration.

The two-stage heating results showed the predicted geometry and heating uniformity can be improved by rotating the powder bed with respect to the electrodes. For the thin ring simulation, the heating uniformity was close to the functionally graded case and did not require multiple function calls to the finite element simulation. Two-stage heating of the longhorn head highlighted the effectiveness of the process where the predicted geometry for the combined configurations resembled a superposition of the two individual configurations. For certain geometries, two-stage heating could improve the part resolution without the need to functionally grade the powder bed.

3.3 Functional Grading with Multiple Electrode Configurations

Implementing a two-stage heating approach improved the uniformity index for uniformly doped geometries. Subsequent simulations were conducted to evaluate whether the uniformity index could be reduced further by combining the two-stage heating process with the heuristic tuning method to functionally grade the electrical conductivity. A diamond geometry with a side length of 3 cm and thickness of 1 cm was chosen to test combined effects, and the electrode configurations are illustrated in Figure 20. The diamond geometry was selected because the vertices were oriented towards the electrodes in both configurations, increasing the likelihood of electric field concentrations and non-uniform heating.

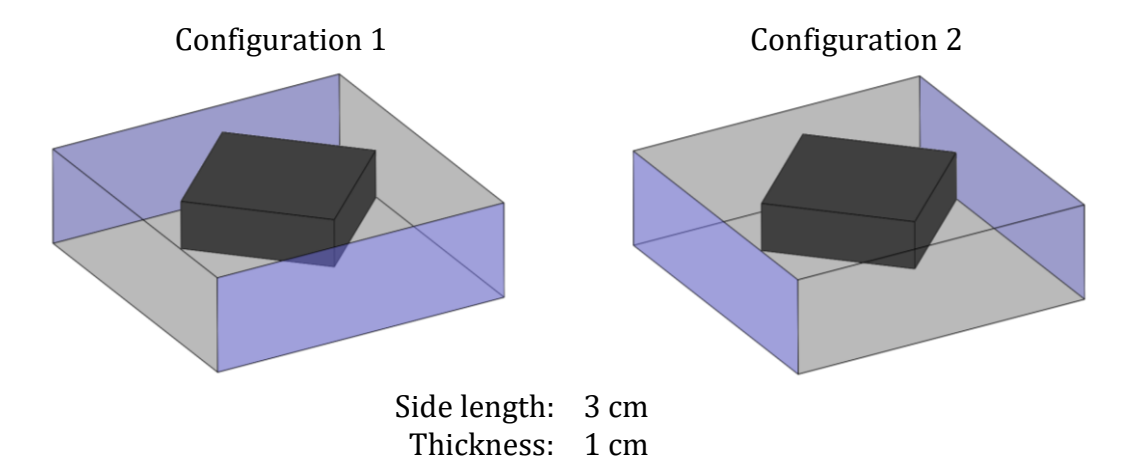


Figure 20 Electrode configurations for orientation-dependent simulations of a diamond

To establish a baseline, the first configuration was used in the heuristic tuning process. The uniformity index for a constant electrical conductivity and single electrode configuration was 0.161. Functional grading with the electrodes in the first configuration improved the uniformity index to 0.125, as shown in Figure 21.

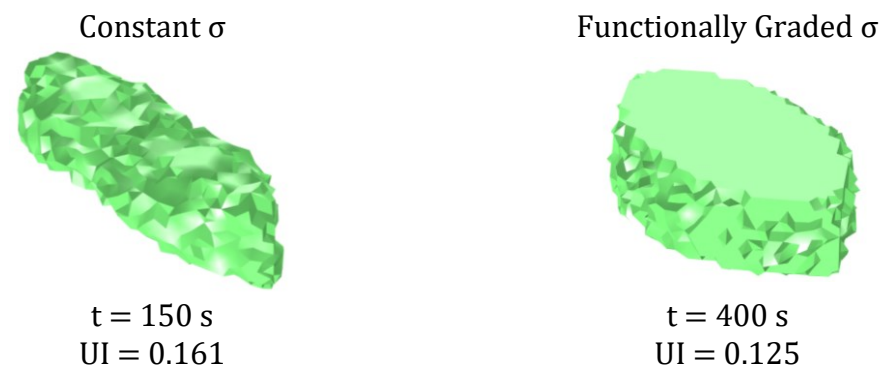


Figure 21 Predicted geometry and uniformity index for single electrode configuration heating and functional grading for the diamond geometry

Next, the two-stage heating mechanism was applied, and the functional grading process was repeated. The predicted geometries and uniformity index values for the constant and functionally graded conductivities are given in Figure 22. Two-stage heating improved the uniformity index compared with the single stage results even after functional grading. The lowest value for the uniformity index was achieved by combining the effects of multiple electrode configurations and heuristic tuning.



Figure 22 Predicted geometry and uniformity index for multiple electrode configurations with (right) and without (left) functional grading for the diamond geometry

The functionally graded electrical conductivity distributions at the center cross section for the single-stage and two-stage electrode configurations are shown in Figure 23. For the single-stage process, very little heating occurred along the sides of the diamond, and the electrical conductivity was tuned to its maximum value in those regions. The pattern for the two-stage process was noticeably different, and the majority of the tuning occurred around the perimeter. As demonstrated in the conductivity distributions and the uniformity index values, functional grading with multiple electrode configurations was the most effective method for improving the heating uniformity in the RF simulations.

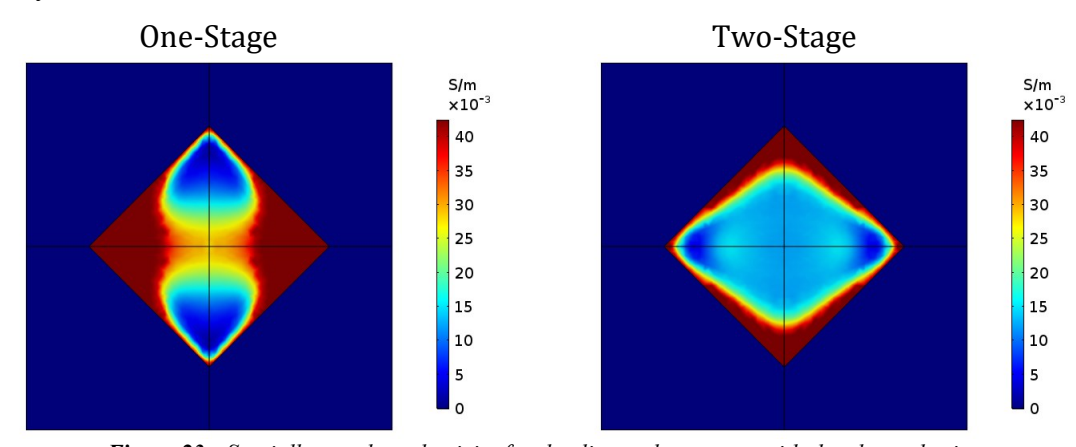


Figure 23 Spatially tuned conductivity for the diamond geometry with the electrodes in the first configuration (left) and multiple configurations (right)

Based on the results of the computational design strategies, certain geometries are likely to benefit from each of the different methods. Functional grading of the powder bed is required when the part geometry differs substantially from a sphere or includes flat faces and corners. Functional grading is most effective when the primary features are aligned with the applied electric field.

Rotating the powder bed to apply the electric field in multiple orientations can improve the heating uniformity for certain geometries without functionally grading the powder bed. Parts that have multiple planes of symmetry such as cubes, cylinders, and rings are particularly suited for this method where functional grading of the powder bed is not required. While symmetric parts are good candidates for powder bed rotation, sharp corners aligned in the direction of the electric field can still cause adverse heating characteristics and should be avoided. For geometries that have multiple corners and planes of symmetry, combining the effects of functional grading with multiple electric field orientations can have the greatest impact on heating uniformity.

4 Conclusion

Finite element analysis simulations in COMSOL Multiphysics® enabled the prediction of temperature rise and phase change behavior of the doped powder beds in an RF-assisted AM process. The models were used to show the electric field concentrations within non-spherical geometries that led to thermal gradients within the parts. Geometrically-induced non-uniform heating was responsible for the unintended curvature seen in the parts produced in the RF heating experiments. A computational design strategy using COMSOL® FEA models was implemented to improve the heating uniformity by functionally grading the electrical conductivity throughout the doped region. The electrical conductivity was spatially graded by applying a heuristic to adjust the conductivity values at every node in the FEA mesh in an iterative process. The design strategy was evaluated according to the relative change in the uniformity of heating (as measured by the uniformity index) before and after tuning. It was also shown that improving the uniformity index led to predicted improvements in the fused geometry. An alternative method to improve the heating uniformity was demonstrated by modifying the orientation of the electric field to simulate a 90 degree rotation of the powder bed during heating. Lastly, the greatest improvement in uniformity index was achieved by combining the effects of functionally grading the electrical conductivity with multiple electric field orientations.

Acknowledgement

This material is based on work supported by the National Science Foundation under Grant No. CMMI-1728015. Any opinions, findings, and conclusions or recommendations expressed in this material are those of the author and do not necessarily reflect the views of the National Science Foundation.

References

- [1] Allison J. Radio frequency additive manufacturing: A volumetric appropach to polymer powder bed fusion. The University of Texas at Austin, 2020. PhD Dissertation.
- [2] Altemimi A, Aziz SN, Al-Hilphy ARS, Lakhssassi N, Watson DG, Ibrahim SA. Critical review of radio-frequency (RF) heating applications in food processing. Food Qual Saf 2019;3:81–91.
- [3] Birla SL, Wang S, Tang J. Computer simulation of radio frequency heating of model fruit immersed in water. J Food Eng 2008;84:270–80.
- [4] Dev SR., Kannan S, Gariepy Y, Vijaya Raghavan GS. Optimization of radio frequency heating of in-shell eggs through finite element modeling and experimental trials. Prog Electromagn Res B 2012;45:203–22.
- [5] Alfaifi B, Tang J, Rasco B, Wang S, Sablani S. Computer simulation analyses to improve radio frequency (RF) heating uniformity in dried fruits for insect control. Innov Food Sci Emerg Technol 2016;37:125–37.
- [6] Jiao Y, Shi H, Tang J, Li F, Wang S. Improvement of radio frequency (RF) heating uniformity on low moisture foods with Polyetherimide (PEI) blocks. Food Res Int 2015;74:106–14.
- [7] Zhao X, Zhao J, Cao J, Wang X, Chen M, Dang Z. Tuning the dielectric properties of polystyrede/poly(vinylidene flouride) blends by selectively localizing carbon black nanoparticles. J Phys Chem 2013;117:2505–15.
- [8] Mehdizadeh M. Electric field (capacitive) applicators/probes.Microwave/RF Applicators and Probes: for Material Heating, Sensing, and Plasma Generation, Waltham, MA: William Andrew; 2015, p. 68–111.
- [9] AC/DC Module User's Guide. Stockholm, Sweden: 2017.
- [10] Kiraly A, Ronkay F. Temperature dependene of electrical properties in conductive polymer composites. Polym Test 2015;43:154–62.
- [11] Heat Transfer Module User's Guide. Stockholm, Sweden: 2017.
- [12] Mokhena TC, Mochane MJ, Sefadi JS, Motloung SV, Andala DM. Thermal conductivity of graphite-based polymer composites. Impact Therm Conduct Energy Technol 2018.
- [13] Vairamohan B, Bran I, Merec de Bellefon G. What's new in electrotechnologies for industrial process heating? ACEEE Summer Study Effic. Ind., Washington, DC: 2011.
- [14] Diller TT, Sreenivasan R, Beaman J, Bourell D, LaRocco J. Thermal model of the build environment for polyamide powder selective laser sintering. Proc. Solid Free. Fabr. Symp., Austin, TX: 2010.
- [15] Ulf H, Rohde-Liebenhau W. Nylon 12. Polym. Data Handb., 1999, p. 225–9.
- [16] Vasquez M, Haworth B, Hopkinson B. Optimum sintering region for laser sintered nylon-12. J Eng Manuf 2011;225:2240–8.
- [17] Yuan M, Diller TT, Bourell D, Beaman J. Thermal conductivity of polyamide 12 powder for use in laser sintering. Rapid Prototyp J 2013;19:437–45.

- [18] Wen J. Heat Capacities of Polymers. Phys. Prop. Polym., 2007, p. 145–54.
- [19] Bannach N. Phase change: cooling and solidification of metal 2014. https://www.comsol.com/blogs/phase-change-cooling-solidification-metal/.
- [20] Bohidar SK, Sharma R, Mishra PR. Functionally graded materials: A critical review. Int J Sci Footprints 2014;2:18–29.
- [21] Mlejnek H. Some aspects of the genesis of structures. Struct Optim 1992;5:64–9.
- [22] Sigmund O. A 99 line topology optimization code written in Matlab. Struct Multidiscip Optim 2001;21:120–7.
- [23] Rozvany G. Aims, scope, methods, and unified terminology of computer-aided topology optimization in structural mechanics. Struct Multidiscip Optim 2001;21:90–108.
- [24] Rozvany G. A critical review of established methods of structural topology optimization. Struct Multidiscip Optim 2009;37:217–37.
- [25] Alfaifi B, Tang J, Jiao Y, Wang S, Rasco B, Jiao S, et al. Radio frequency disinfestation treatments for dried fruit: Model development and validation. J Food Eng 2014;120:268–76.
- [26] Birla SL, Wang S, Tang J, Hallman H. Improving heating uniformity of fresh fruit in radio frequency treatments for pest control. Postharvest Biol Technol 2004;33:205–17.